

Letter of Intent for the J-PARC 50 GeV PS  
**Measurement of X rays from  $\Xi^-$  C atom  
with an active fiber target system**

T. O. Yamamoto, M. Fujita, K. Tanida  
*Japan Atomic Energy Agency (JAEA), Japan*

Y. Ishikawa, K. Kamada, T. Koike, F. Oura, H. Tamura  
*Tohoku University, Japan*

M. Ukai  
*High Energy Accelerator Research Organization (KEK), Japan*

### Abstract

We propose to perform a measurement of  $\Xi^-$ -atomic X rays from a carbon target at the K1.8 beam line to study Baryon-Baryon interaction in the  $S = -2$  sector. We have limited data for this sector so far. X-ray spectroscopy of hadronic atoms give us various information on the strong interaction between hadrons and nuclei. X-ray energy shift and width give information on the real part and the imaginary part of the optical potential in nuclei. This method had been successfully applied in cases of negative charged hadrons. Now, the same method will be applied to  $\Xi^-$  atoms on various target nuclei over wide mass range in J-PARC experiments.

In this proposed experiment, a carbon target was selected because of a technical reason and an additional motivation related to the emulsion data for  $S = -2$  bound systems. Furthermore, we have a chance to obtain a part of data for  $\Xi^-$ -atomic X rays in an approved experiment J-PARC E70, expected to be run in 2023. X-ray data can be taken in parallel with the E70 data-taking by installing a high-resolution X-ray detector system (modified Hyperball-X) near the E70 target, an active fiber target (AFT). Other apparatus are common with J-PARC E70. Hyperball-X is a Germanium(Ge) detector array of which performance was well established in the previous X-ray measurements in J-PARC E03 and E07. For a good signal to noise ratio in the X-ray spectrum, track information of AFT will be used for tagging  $\Xi^-$  stop.

We are aiming for the first data taking (phase-1) of this proposed experiment in parallel with J-PARC E70 to confirm yields of X rays from  $\Xi^-$  C atoms. We have a chance to observe the X-ray transitions assuming the X-ray yields and the natural width of the  $\Xi^-$ -atomic state suggested by a theoretical calculation. However, there are large uncertainties on the yields and the width due to unknown absorption strength. We will reconsider about additional beam time (phase-2) to obtain finite energy shifts and widths after the phase-1 data taking.

# 1 Physics motivation

Strangeness nuclear physics in the  $S = -2$  sector is one of the biggest motivation for the J-PARC 50 GeV proton synchrotron. This is a significant step forward from  $S = -1$  system towards the multi-strangeness hadronic systems, where interactions between hyperons may play an important role. The interactions between two hyperons with strangeness first appear in the  $S = -2$  systems. In addition, in the  $S = -2$  sector, strong coupling between  $\Xi N$  and  $\Lambda\Lambda$  is expected because the mass difference is as small as 28 MeV, which is much smaller than the case of  $S = 0$  and 1 sector. Thus, the  $S = -2$  system may be the first system where the baryon coupling effect may plays a dominant role.

Furthermore, understanding of the  $\Xi N$  interaction is essential to know a role of  $\Xi^-$  in neutron stars, where high-density condition, the density of 2–3 times the nuclear saturation density ( $\rho_0$ ), is believed to be realized in the core. In this condition, the strangeness degrees of freedom should play an essential role because the neutron Fermi energy would become larger than the mass difference between hyperons and a nucleon. Especially, there are negative charged hyperons ( $\Sigma^-$  and  $\Xi^-$ ), with s quarks having negative charge of  $-1/3e$ , which can reduce the electron Fermi energy by considering the charge neutrality.  $\Sigma^-$ s would not appear in neutron stars due to strongly repulsive potential,  $U_\Sigma \sim +30$  MeV. The next candidate is  $\Xi^-$  which is interested in the proposed experiment. It is awaited to have a good estimate of the  $\Xi^- N$  potential from experimental results.

However, little is known experimentally on  $S = -2$  systems, especially  $\Xi N$  system. While some emulsion events of  $\Xi^- + \text{nuclei}$  system have been reported [1], it is still not conclusive for understanding of the  $\Xi N$  interaction. Some upper limits on the  $\Xi$ -nucleus potential have been obtained from the production rate and spectrum shape in the bound region of  $\Xi$ -hypernucleus via the  $^{12}\text{C}(K^-, K^+)$  reaction in the BNL E885 experiment [2]. In this experiment,  $\Xi$ -hypernuclear states were not clearly observed because of the limited statistics and detector resolution. The experimental group suggested an attractive  $\Xi$  potential with a depth of about 14 MeV for  $A = 12$  assuming Woods-Saxon type potential shape, but the derivation of the potential was model dependent and was not conclusive. In this situation, clear observation of  $\Xi$ -hypernuclear states will play an important role for the  $S = -2$  system.  $\Xi$ -hypernuclei give valuable information on the  $S = -2$  baryon-baryon effective interactions such as  $\Xi N$ , and  $\Xi N \rightarrow \Lambda\Lambda$ . In near future, a  $\Xi^-$  hypernuclear spectroscopic experiment via the  $^{12}\text{C}(K^-, K^+)$  reaction will be performed in J-PARC E70 with much improved energy resolution [3].

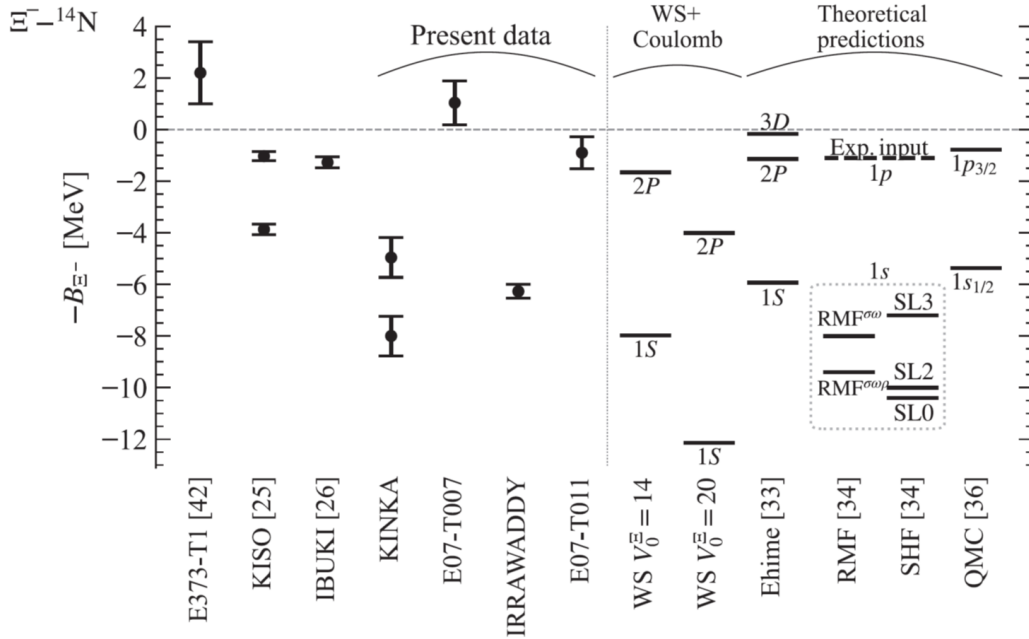


Figure 1:  $B_{\Xi^-}$  for the  $\Xi^- - ^{14}\text{N}$  system of the emulsion events found in KEK E373 and J-PARC E07 and theoretical calculations [1].

## Recent progress in study of the $\Xi N$ interaction

Recently, some experimental results have been reported on the  $\Xi N$  interaction. From the emulsion experiments, KEK E373 and J-PARC E07, observations of some special events were reported such as double  $\Lambda$  hypernucleus [4] and  $\Xi$  hypernuclei [1, 5]. The measured binding energies ( $B_{\Xi^-}$ ) for  $\Xi^- - ^{14}\text{N}$  systems are summarized in Fig. 1. In the case of "KINKA" and "IRRAWADDY" events, decay of  $\Xi^- - ^{14}\text{N}$  systems were observed with derived  $B_{\Xi^-}$  of  $8.00 \pm 0.77$  MeV or  $4.96 \pm 0.77$  MeV and  $6.27 \pm 0.27$  MeV, respectively. These  $B_{\Xi^-}$  values are significantly larger than that of the  $1p$  state. Thus, these events are attributed to the  $1s$  state, namely the ground-state spin-doublet ( $3/2^+$ ,  $1/2^+$ ) of the  $^{15}_{\Xi}\text{C}$  hypernucleus. The observation of the  $1s$  state may indicate a weak absorption strength. The emulsion analysis is now on-going and it is expected to find more events like the "IRRAWADDY" event which may clarify the energy and the width of the  $1s$  and the  $1p$  states.

The ALICE experimental group reported their result related to the  $p - \Xi^-$  strong interaction by using two-particle  $p - \Xi^-$  correlation from  $p$ -Pb collisions with  $\sqrt{s_{NN}} = 5.02$  TeV, this method is called "femtoscopy" [6]. Since the measured  $p - \Xi^-$  correlation is significantly enhanced with respect to the only Coulomb prediction, the presence of an additional  $p - \Xi^-$  attractive interaction is suggested. The data are compatible with recent lattice calculations by the HAL-QCD Collaboration.

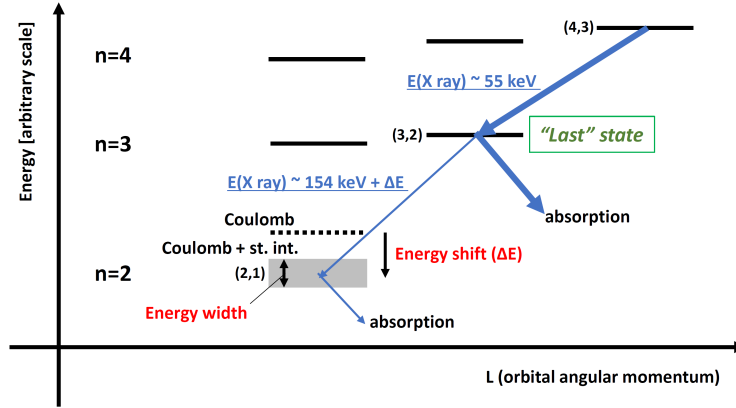


Figure 2: Level scheme of  $\Xi^-$  C atom.

For theoretical studies, the Nijmegen group has constructed various baryon-baryon interaction models based on one boson exchange picture. Most of the models predict a repulsive  $\Xi N$  interaction, while a recent model called ESC16 presented an attractive  $\Xi N$  interaction [7]. HAL QCD group has started to provide baryon-baryon interactions with lattice QCD method. Recently, a lattice QCD calculation near the physical point presented a  $\Xi N$  potential [8] which shows much weaker  $\Xi N - \Lambda\Lambda$  term. Chiral effective field theory is also a powerful new tool for understanding hadronic interactions. The recent study presented properties of the  $\Xi^-$  in the nuclear medium at the next-to-leading-order level [9].

## X-ray spectroscopy of $\Xi^-$ C atom

Because of limited knowledge obtained from experimental results, there is no established interaction model in  $S = -2$  channels. Various models [10, 11, 12] estimated the depth of the  $\Xi A$  optical potential. However, the derived potential are different among interaction models which demonstrates that the experimental information on  $U_{\Xi}$  is crucially important in order to discriminate reasonable interaction models.

Here, we propose the measurement of X rays from a  $\Xi$  atom to obtain information on the  $\Xi N$  interaction. X-ray spectroscopy of hadronic atoms give us various information on strong interaction between hadrons and nuclei. This method had been successfully applied in cases of negative charged hadrons ( $\pi^-$ ,  $K^-$ ,  $\bar{p}$ , and  $\Sigma^-$ ). Negative charged hadrons can come close to nuclear surface leading energy shifts on atomic states by strong interaction as well as energy widths by absorption. Therefore, the X-ray energy shift and width give information on the real and the imaginary part of optical potential. In the  $S = -1$  sector, for example, more than twenty data points are available for  $\Sigma^-$  atoms on wide mass range nuclei which give constraint on  $\Sigma^-$ -nuclei optical potentials [13]. On the other

hand, no experimental data for  $\Xi$ -atomic X ray exists at present. We are aiming for measurement of X rays from  $\Xi^-$  atoms on various target nuclei over wide mass range and have conducted two experiments, J-PARC E07(2016-2017) and J-PARC E03(2020-2021). Analysis of these experiments is on-going and we will report the results in near future.

In this proposed experiment, a carbon target was selected because of a technical reason and an additional motivation related to the emulsion data for  $S = -2$  bound systems discussed below. Furthermore, we have a chance to obtain a part of data for  $\Xi^-$ -atomic X rays from the carbon target in an approved experiment as described in section 2. In the proposed experiment, we will measure two X-ray transitions of  $(n, l) = (4, 3) \rightarrow (3, 2)$  and  $(3, 2) \rightarrow (2, 1)$  from  $\Xi^-$  C atoms, corresponding X-ray energies are  $\sim 55$  keV and  $\sim 155$  keV, respectively. Figure 2 shows a level scheme of the  $\Xi^-$  C atom. The finite energy shift and natural width would be appeared in the  $(2, 1)$  state. By measuring the energy shift and width and comparing them with expected values with only Coulomb interaction, we can obtain information of the real and the imaginary part of the  $\Xi A$  optical potential. Because of a large absorption probability in the  $(2, 1)$  state, no X ray is expected to be emitted from the state. Furthermore, because the  $(3, 2)$  state would also have absorption probability, the yield of the X rays of the "lower" transition  $(3, 2) \rightarrow (2, 1)$  should be smaller than that of the "upper" transition  $(4, 3) \rightarrow (3, 2)$ . This yield ratio of the "upper" and the "lower" transitions also have information of the imaginary part of the potential. A preliminarily theoretical study for the X rays from  $\Xi^-$  C atoms using cascade model calculation suggest the energy shift ( $\Delta E$ ) and the width ( $\Gamma$ ) of the  $(2, 1)$  state to be  $\Delta E > 1$  MeV and  $\Gamma \sim 270$  keV with the ND potential and  $\Delta E \sim 90$  keV and  $\Gamma \sim 6$  keV with the HAL potential [14]. The calculation also suggest an expected yield ratio of the "upper" and the "lower" transitions to be  $1/3$  with the ND potential and almost the same with the HAL potential. Because there are large differences in suggested shifts and widths depending on potentials, experimental data on  $\Xi^-$  C atomic X rays may give a strong constraint to distinguish interaction models.

## Impact on emulsion data

$\Xi$ -atomic X-ray data for light nuclei may have another impact on the emulsion data, such as "NAGARA" event which gives the binding energy of double  $\Lambda$ s ( $B_{\Lambda\Lambda}[\Lambda\Lambda^6\text{He}]$ ) of  $6.91 \pm 0.16$  MeV [15]. In this analysis, the binding energy of  $\Xi^-$  C atom ( $B_{\Xi}$ ) is necessary to obtain  $B_{\Lambda\Lambda}$  value from kinematics at the production point of  $\Lambda\Lambda^6\text{He}$ .  $B_{\Xi}$  of 0.13 MeV, corresponding to the binding energy of  $(3,2)$   $\Xi$ -atomic state, was adopted according to a theoretical suggestion. However, the "last"  $\Xi^-$  C atomic state, having highest  $\Xi^-$  absorption probability per  $\Xi^-$  stop, may be changed if the absorption strength is different from the expectation. The absorption strength, thus which state is "last", should be confirmed by  $\Xi$ -atomic X-ray spectroscopy.  $\Xi$ -atomic X-ray data for nuclei contained in

the emulsion (Carbon, Nitrogen and Oxygen) may help for the emulsion analysis.

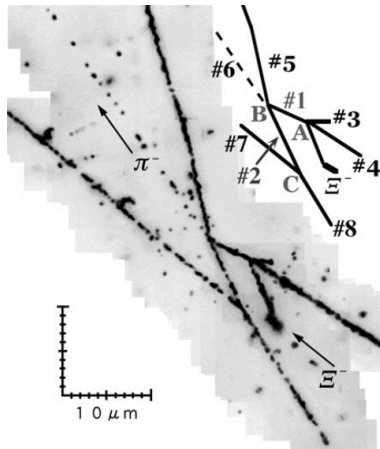


Figure 3: Emulsion image of NAGARA event [15]. This event shows production and decay of a double  $\Lambda$  hypernucleus,  ${}_{\Lambda\Lambda}{}^6\text{He}$ ;  $\Xi^- + {}^{12}\text{C} \rightarrow {}_{\Lambda\Lambda}{}^6\text{He} + {}^4\text{He} + t$ ,  ${}_{\Lambda\Lambda}{}^6\text{He} \rightarrow {}^5_{\Lambda}\text{He} + p + \pi^-$ .

## 2 Strategy of $\Xi^-$ C atomic X-ray measurement

We had tried to measure X rays from  $\Xi^-$  carbon atoms in J-PARC E07 [2016-2017], systematic study of double strangeness system with an emulsion-counter hybrid method [17]. Details of the measurement are shown in Appendix A.1. No clear peak structure was found in X-ray spectra and only upper limit of X-ray yield per  $\Xi^-$  stop was obtained. The preliminary result shows upper limit of  $\sim 0.4$  (assuming the energy width of 1 keV in X-ray energy region of 100-200 keV). This value is almost the same as a theoretical case study with the Lattice QCD potential [14],  $\sim 0.4 / \Xi^-$  stop. Technical reasons of the limited sensitivity for the X-ray measurement are follows; (1) the beam  $K^-$  intensity was limited for smaller contamination of  $\pi^-$  in the beam which make dummy tracks in the nuclear emulsion, (2) acceptance of a X-ray detector (a Ge detector array, Hyperball-X) was limited due to interferences with the emulsion and its mover system and (3) no direct constraint for selecting  $\Xi^-$  stop events, where we applied a rejection with information of a forward counter and a kinematic selection for low momentum  $\Xi^-$ s.

We will retry the measurement for  $\Xi^-$  C atoms with an improved sensitivity in the proposed experiment. X-ray measurement using the same type Ge detector array combined with an Active Fiber Target (AFT) system can improve disadvantages in the previous measurement, namely (1) higher beam intensity can be used without the emulsion, (2) Ge detectors can be closer to the target thanks to a cross shape of AFT and (3) track information of AFT can be used for the  $\Xi^-$  stop selection. We have a chance to take

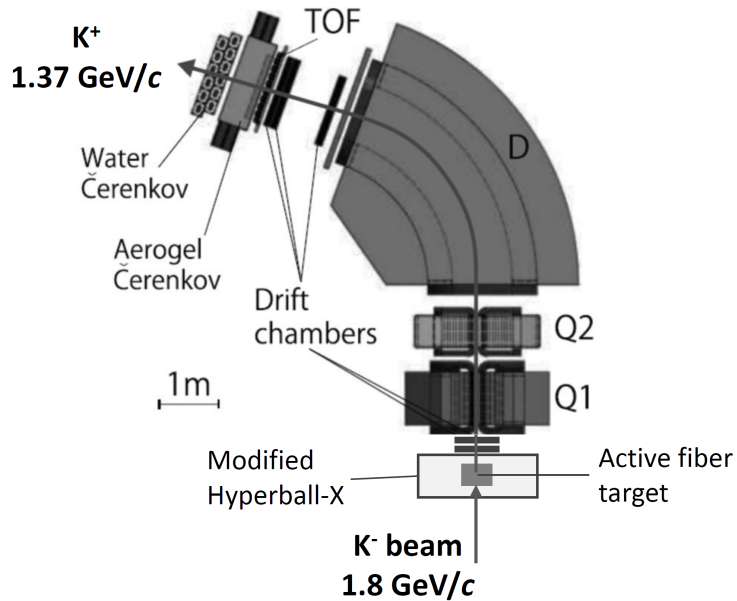


Figure 4: Experimental setup of the proposed experiment.

data of  $\Xi^-$  C atomic X rays in parallel with J-PARC E70, spectroscopic study of  $\Xi^-$  hypernucleus with the S-2S spectrometer [3], in which an active fiber target system will be installed for an energy loss correction. It is expected that peak structures of the X rays from  $\Xi^-$  C atoms will be observed with the the number of  $K^-$  beams requested for J-PARC E70, while an accuracy on the energy shift and width is not sufficient due to limited statistics. In addition, there are large uncertainties on the X-ray yield estimation as described in section 4. Therefore, we are considering two phase data-taking for the proposed experiment, the phase-1 for observation of X rays from  $\Xi^-$  C atoms to obtain realistic X-ray yield estimation and the phase-2 for measurement of the finite energy shifts and widths. The phase-1 data-taking can be done in the J-PARC E70 beam time. After an analysis of the phase-1 data, we will reconsider about necessary beam time for the phase-2 data-taking and report it in the PAC meeting.

### 3 Experimental method and detector system

The proposed experiment will be performed at the K1.8 beam line together with the Beamline spectrometer, the S-2S spectrometer and an Ge detector array, modified Hyperball-X. Figure 4 shows a schematic view of the experimental setup. The setup is common with the J-PARC E70 except for the modified Hyperball-X.

$\Xi^-$  is produced by the  $(K^-, K^+)\Xi^-$  reaction at 1.8 GeV/c where the cross section of the elementary process,  $p(K^-, K^+)\Xi^-$ , is at maximum as shown in Fig.5. Beam  $K^-$ s and scattered  $K^+$ s are particle identified and momentum analyzed by magnetic spectrometers,

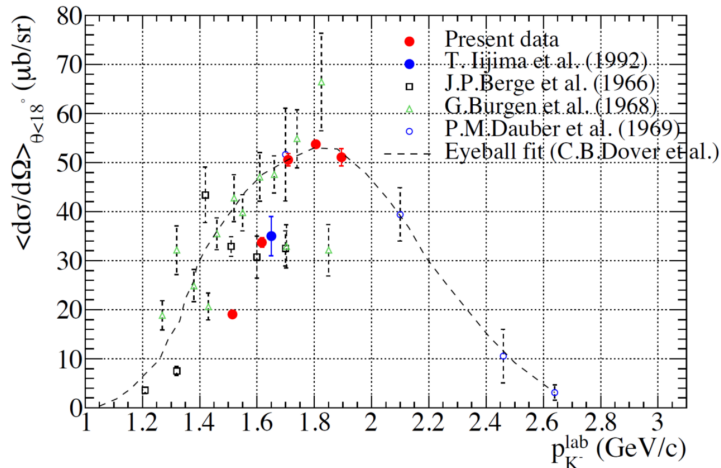


Figure 5: the cross section of the elementary process,  $p(K^-, K^+)\Xi^-$  as a function of beam  $K^-$  momentum [16].

the Beamline spectrometer and the S-2S spectrometer, respectively. Details of them are shown in section 3.1 and 3.2. Events of  $\Xi^-$  productions will be selected by a missing-mass analysis based on measured momenta in the Beamline and S-2S spectrometers. A missing-mass resolution better than 30 MeV is enough for a tagging of  $\Xi^-$  productions as in the case of the previous  $\Xi^-$ -atomic X-ray spectroscopy (J-PARC E03) using KURAMA spectrometer described in Appendix A.2. Therefore, The Beamline and S-2S spectrometer system, in which an expected missing-mass resolution is better than 2 MeV, has sufficient performance for this measurement. For X-ray detection, Hyperball-X, which was used in the previous  $\Xi^-$ -atomic X-ray spectroscopy J-PARC E07 and E03, will be installed with modified geometrical configuration considering interferences with a target system. Details are shown in section 3.3. Active Fiber Target (AFT) will be used as a carbon target of which track information can be used for the  $\Xi^-$  stop identification. Details of the AFT system are shown in section 3.4. Description of a trigger and a data-acquisition (DAQ) system is also shown in section 3.5.

### 3.1 K1.8 beam line and Beamline spectrometer

The J-PARC K1.8 beam line was constructed to carry out missing-mass spectroscopy of hypernuclei both for  $S = -1$  and  $-2$  sectors and exotic hadrons. Secondary meson beams are produced at a primary target (Au, 66 mm thickness) placed at the most upstream in Hadron Experimental Facility by irradiating proton beam from J-PARC 30-GeV synchrotron. Secondary beams are delivered to the K1.8 beam line which was designed to provide separated pions and kaons with the momentum up to  $\sim 2$  GeV/ $c$  having  $\sim 3\%$  momentum bite. For the kaon beam, good  $K/\pi$  separation with reasonable

intensities is realized by removing pion contamination using two electrostatic separators (ESS1, ESS2) with a length of 6 m each and with mass slits installed at downstream of each separator. Furthermore, intermediate focus (IF) slits reject cloud pions generated near the primary target. The length between the primary target and the experimental target is  $\sim 46$  m. We conducted beam optics tuning in the previous experiment J-PARC E42 performed in 2021. With the optimized beam line magnet parameters, the  $K^-$  intensity at the experimental target was  $\sim 800 \times 10^3$  per spill for  $p_K = 1.8$  GeV/ $c$  with 64kW MR operation.  $K/\pi$  ratio was measured to be 1:1 with this condition.

For the momentum-analysis of beam particles, the beamline spectrometer consists of QQDQQ magnets, with detectors for tracking (a scintillation fiber counter[BFT], drift chambers [BC3,4]). This system is completely common with the setup for J-PARC E70. The incident  $K^-$  momentum will be reconstructed using a third-order beam transport matrix with a hit position in BFT at the upstream of the magnets and a straight track measured by BC3 and BC4 at the downstream. The designed momentum resolution is  $3.3 \times 10^{-3}$  (FWHM) with the position accuracy of 0.2 mm (rms) for a measured beam trajectory. For the particle identification, time-of-flight analysis is applied using a time difference between BH1 and BH2, installed at up- and down-stream of the QQDQQ magnets, respectively. BH1 and BH2 are plastic scintillation counters which are horizontally segmented. An aerogel Cherenkov counter (BAC) will be installed for generating a data-taking trigger.

Details of the detector are described in [18, 19]. The detector system is already exists at the K1.8 beam line and well established in the previous experiments.

### 3.2 S-2S spectrometer

The  $K^+$ s scattered at forward angle from the  $(K^-, K^+)$  reaction are momentum analyzed with the S-2S spectrometer. This system is also completely common with the setup for J-PARC E70. The spectrometer consists of two quadrupole magnets and one dipole magnet (QQD). The first quadrupole magnet focuses the particles in vertical, and the next one in horizontal. A large aperture of the two quadrupole magnets keeps the solid angle as large as 55 msr. The bending angle for the central momentum of the dipole magnet is 70 degrees at 1.37 GeV/ $c$ , which is typical value for  $K^+$  produced in the  $(K^-, K^+)$  reaction with a 1.8 GeV/ $c$  beam. The momentum acceptance of the S-2S is 1.2–1.6 GeV/ $c$ . For lower ratio of the  $K^+$ 's decay in flight, the flight length is kept as short as 9 m with a survival rate of 40%. The momentum resolution of the S-2S is estimated from a simulation and found to be  $5.5 \times 10^{-4}$  (FWHM) by assuming the position resolution of drift chambers to be 250  $\mu\text{m}$ .

For the momentum analysis, the trajectory of scattered  $K^+$ s will be reconstructed based on position information measured by the drift chambers at upstream (SDC1,2) and down-

stream (SDC3–5) of the QGD magnets using the magnetic field distribution calculated by the TOSCA code with corrections based on a measured magnetic field. These detectors have effective areas wide enough to cover the scattered particle profile. The S-2S pole gap will be filled with He gas contained in a bag with 16  $\mu\text{m}$ -thick Mylar windows to reduce multiple scattering. For the particle identification, time-of-flight analysis is applied using a time difference between BH2 and TOF. TOF is a plastic scintillation counter which is horizontally segmented. Counters for generating a data-taking trigger will be installed: an aerogel Cherenkov counter (AC: refractive index  $n=1.055$ ) for  $\pi^+$  veto, and a water Cherenkov counter (WC:  $n=1.33$ ) for proton veto.

Installation of the S-2S magnet system to the K1.8 beam line will be done in early 2022 and their detectors will be ready by fall 2022.

### 3.3 Modified Hyperball-X (Hyperball-X')

X rays will be detected by a Ge detector array by taking a coincidence with magnetic spectrometers. The Ge detector array, modified Hyperball-X, will be installed near the target. Modified Hyperball-X consists of four Clover-type Ge detector and two Single-type Ge detector, equipped with  $\text{Bi}_4\text{Ge}_3\text{O}_{12}$  (BGO) suppressors surrounding each Ge crystal to suppress background events such as Compton scattering and high energy photons from  $\pi^0$  decay. Components of the array is almost common with a Ge detector array (Hyperball-X) used in the previous experiments J-PARC E07[2016-2017] and E03[2020-2021]. As shown in Fig. 6(a), the detector configuration of modified Hyperball-X is arranged so as to avoid interferences between Hyperball-X detectors, trigger counters and the AFT system. Clover-type Ge detectors were installed at corner positions of the AFT system for a large solid angle and a low counting rate of each Ge crystal. Single type detector will be installed at up-stream side of the target where the counting rate is expected to be not serious. Photo-peak efficiencies for the array are estimated based on a Monte-Carlo simulation using the GEANT4 code as shown in Fig. 6(b). The plots shows the efficiency curve as a function of a X-ray energy with and without an effect of self-absorption inside the target. The photo-peak efficiencies are expected to be 3.9% and 3.8% for 55 keV and 155 keV, respectively. With this configuration, modified Hyperball-X will not affect the performance of the AFT system, thus no effect is expected for the main purpose of J-PARC E70.

High energy resolution has great merit for the small ( $<1$  keV) energy width case, even if dead time due to signal pileups become longer. To optimize for a beam intensity of 0.5–1 MHz, slow type shaping amplifiers, ORTEC 671, will be used for the modified Hyperball-X, while fast type shaping amplifiers should be used for a higher beam intensity. In the previous experiment J-PARC E03, a typical energy resolution was  $\sim 2$  keV (FWHM) for 202 keV.

A  $\text{Lu}_2\text{SiO}_5$  (LSO) scintillator will be installed adjacent to each of the Ge detectors and used as a triggerable calibration source, it is called "LSO pulser". The crystal contains  $^{176}\text{Lu}$ , with a natural abundance of 2.6%, which emits 202 keV and 307 keV  $\gamma$  rays. The LSO pulser provides a timing signal for  $\gamma$ -ray emissions from  $^{176}\text{Lu}$  by detecting a  $\beta$  ray. Through a  $\beta - \gamma$  coincidence measurement between a LSO pulser and a Ge detector, we can discern  $\gamma$  rays from  $^{176}\text{Lu}$  efficiently even in the in-beam condition. Data taken during beam spill and off the beam spill will be used for an energy calibration and a monitoring of the performance of the Ge detectors over the beam time. In the previous experiments J-PARC E07 and E03, this method was successfully applied with an accuracy of the energy calibration of 0.05 keV.

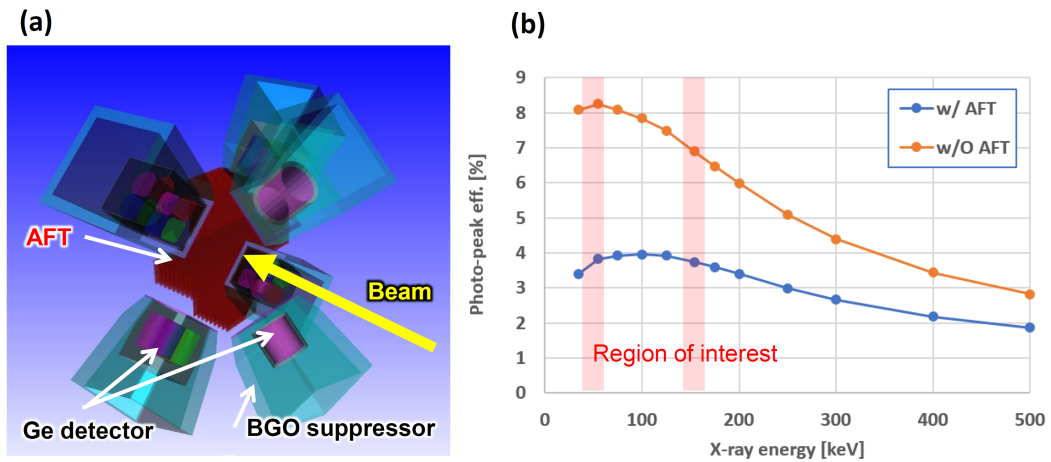


Figure 6: Schematic view of a Ge detector array (modified Hyperball-X) (a) and its photo peak efficiencies (b).

### 3.4 Active Fiber Target (AFT)

In J-PARC E70, spectroscopic study of  $\Xi^-$  hypernucleus with the high resolution S-2S spectrometer, a  $9 \text{ g/cm}^2$  thick target will be used to gain yield of  $\Xi$  hypernuclei, of which production cross section is small, reported to be  $89 \pm 14 \text{ nb/sr}$  for the angular average from  $0^\circ$  to  $8^\circ$  from the BNL AGS-E885 experiment [2]. Therefore, the Active Fiber Target (AFT) system is introduced to achieve a good missing-mass resolution of better than 2 MeV(FWHM) required for the purpose of J-PARC E70 by measuring actual energy losses inside the target. The AFT is made of scintillating fibers. As shown in Fig. 7(a), we will use  $\phi 3 \text{ mm}$  scintillation fibers (Saint-Gobain, BCF-10SC) to make the net target size of  $5\text{cm}[\text{H}] \times 10\text{cm}[\text{W}] \times 10\text{cm}[\text{T}]$ . By recording the pulse height of each scintillation fiber via MPPCs with EASIROC modules, we can correct the energy loss for tracks of beam  $K^-$ s

and scattered  $K^+$ s. Thus we can keep the energy resolution better than 2 MeV(FWHM) even with a thick target.

For the X-ray measurement, track information of AFT can be used for tagging  $\Xi^-$  stop events, namely tracks of  $\Xi^-$ s produced via the  $(K^-, K^+)$  reaction end inside the target region followed by reaction vertexes due to  $\Xi^-$  absorption into a carbon nuclei. With this selection, we can reject dominant background sources such as (1)  $\Xi^-$ s pass through and exit the target and (2)  $\Xi^-$ s decay in-flight inside. Detailed analysis procedure will be discussed based on a Monte Carlo simulation in near future.

A part of AFT system had been constructed as shown in Fig. 7(b) and its performance was evaluated in test experiments at RCNP and ELPH [16]. It was found that the energy resolution of the fiber is  $\Delta E/E = 10\%$  at  $\Delta E = 0.7$  MeV which corresponds to a mean value of energy loss of kaons in J-PARC E70. Full set of AFT will be constructed near future and installed to the K1.8 beam line in fall 2022.

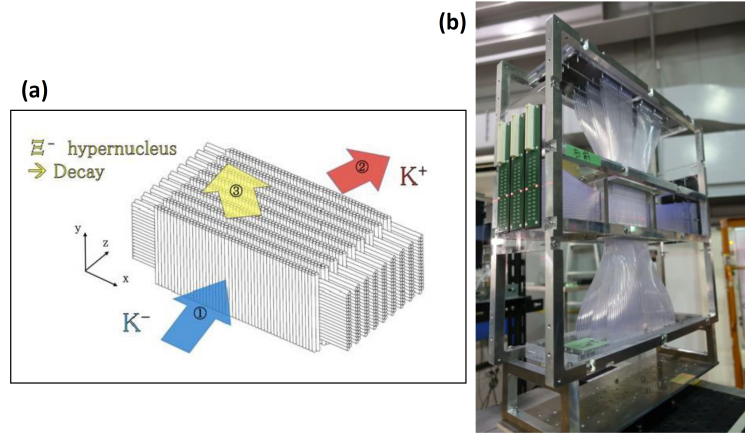


Figure 7: Schematic view of Active Fiber Target (a) and photo of a part of AFT for test experiments (b).

### 3.5 Trigger and Data acquisition system

To select true  $(K^-, K^+)$  reaction events from a large amount of backgrounds such as  $(K^-, \pi^+)$  events, a data-taking trigger will be constructed by using information of trigger counters: plastic scintillation counters (BH1, BH2, TOF), aerogel Cherenkov counters (BAC, AC) and a water Cherenkov counter (WC).  $K^-$  beam trigger and out-going  $K^+$  trigger are generated as " $BH1 \times BH2 \times \overline{BAC}$ " and " $TOF \times \overline{AC} \times WC$ ", respectively. This system is common with that for J-PARC E70. The expected trigger rate is less than 200 counts/spill as described in the technical design report of J-PARC E70 [16]. The DAQ efficiency is expected to be more than 95% with this trigger rate.

DAQ system and components for magnetic spectrometers will be almost same as those used for the previous experiment J-PARC E40 [2018-2020] and common with J-PARC E70. Network oriented readout modules, HUL and EASIROC, will be integrated by a network-based data-taking system (HD-DAQ) [20]. Data from each module are gathered by controllers having network interfaces with TCP/IP protocol. Event matching for data from each module will be controlled by MTM/RM system.

For the X-ray measurement, an independent DAQ system for readout of the modified Hyperball-X (Ge detectors and BGO counters) will be constructed. ADC/TDC data will be gathered to HUL modules and then to a host computer. This system is the same as the previous X-ray measurement in J-PARC E03. A dead time of this DAQ system is almost same as that for the magnetic spectrometers. An event matching procedure between DAQ systems of the magnetic spectrometers and modified Hyperball-X is common with and had been evaluated in the previous experiment J-PARC E07. This independent DAQ system for the modified Hyperball-X have no effect on the DAQ system for the magnetic spectrometers.

## 4 Expected result

### 4.1 Expected X-ray yield

Expected X-ray yields in the phase-1 data-taking of the proposed experiment are shown in this section. Here, we assume a number of  $K^-$  beams expected in J-PARC E70, corresponding to 20 days beam time with 83kW MR operation. The X-ray yield  $N_X(4 \rightarrow 3)$  for the "upper"  $(n, l) = (4, 3) \rightarrow (3, 2)$  transition is estimated to be 30 counts in the following way.  $N_X(4 \rightarrow 3)$  can be written as

$$N_X(4 \rightarrow 3) = N_{stopped \Xi^-} \times R_X \times \eta_X \times \epsilon_X,$$

where

$N_{stopped \Xi^-}$ : Number of stopped  $\Xi^-$  in the target.

$R_X$ : Intensity of the X ray of interest per stopped  $\Xi^-$ .

$\eta_X$ : Probability that the X ray passes through the target uninteracted.

$\epsilon_X$ : X ray detection efficiency of the modified Hyperball-X.

and  $N_{stopped \Xi^-}$  can be represented by

$$N_{stopped \Xi^-} = N_{beam} \times N_{target} \times \sigma_{\Xi^-} \times \Omega_{K^+} \times \epsilon_{K^+} \times \epsilon_{others} \times R_{\Xi^-}$$

where

$N_{beam}$ : Number of total  $K^-$  beam ( $3.1 \times 10^{11}$ ).

$N_{target}$ : Target thickness ( $4.3 \times 10^{23}$  atoms/cm<sup>2</sup> for both C and H).

- $\sigma_{\Xi^-}$ : Differential cross section of the  $(K^-, K^+)\Xi^-$  reaction.
- $\Omega_{K^+}$ : Acceptance of the S-2S spectrometer (55 msr).
- $\epsilon_{K^+}$ : Overall efficiency of  $K^+$  detection system.
- $\epsilon_{others}$ : Overall efficiency due to DAQ deadtime and trigger efficiency.
- $R_{\Xi^-}$ : Stopping probability of produced  $\Xi^-$ .

Estimation of the parameters are explained in the following.  $\sigma_{\Xi^-}$  for a carbon target can be taken from Ref. [21] as  $38 \times A^{0.38} \mu\text{b/sr}$  and is about  $134 \mu\text{b/sr}$ . That for hydrogen target can be taken as  $52 \mu\text{b/sr}$  as shown in Fig. 5.  $\epsilon_{K^+}$  is estimated to be 0.4, including the effect of  $K^+$  decay loss, based on the estimation for J-PARC E70 because of the common  $K^+$  detecting system (S-2S).  $\epsilon_{others}$  is assumed to be 0.8. Therefore, the number of produced  $\Xi^-$  is  $3.4 \times 10^5$  by summing contributions from both carbon and hydrogen in the target.  $R_{\Xi^-}$  is estimated to be 1.2% by a GEANT4 simulation. Therefore,  $N_{stopped \Xi^-}$  is estimated to be  $4.1 \times 10^3$ .

There are uncertainties in estimating  $R_X$  in the calculation of cascade process in the  $\Xi^-$  atom. According to a calculation [14],  $R_X$  for the transition  $(4, 3) \rightarrow (3, 2)$  in  $\Xi^-$  C atom is 0.3–0.4. We take  $R_X = 0.3$  for this yield estimation.  $\eta_X \times \epsilon_X$  are estimated by a GEANT4 simulation to be 3.9% and 3.8% for 55 keV and 155 keV X rays, respectively. In addition, in-beam deadtime of the Ge detectors should be included in the  $\epsilon_X$ . From our experience in the previous measurement (J-PARC E03, 2020-2021), the dead time is estimated to be 0.7. Therefore,  $\eta_X \times \epsilon_X$  is expected to be  $0.039 \times 0.7 = 0.027$ . By considering these efficiencies, we obtained the expected yield of the "upper" transition ( $\sim 55$  keV) to be  $N_X(4 \rightarrow 3) = 30$  counts.

For the the "lower" transition  $(3, 2) \rightarrow (2, 1)$  of  $\Xi^-$  C atom, there are very large uncertainties in estimating  $R_X$  because it depends on the absorption potential we want to know. Theoretical calculation shows the branching ratio of 30–100% for the X-ray transition  $(3, 2) \rightarrow (2, 1)$  depends on potentials. Therefore, we take the branching ratio of 50% corresponding to  $R_X$  of 0.15. The yields of the transition  $(3, 2) \rightarrow (2, 1)$  ( $\sim 155$  keV) can be calculated to be  $N_X(3 \rightarrow 2) = 15$  counts.

## 4.2 Expected sensitivity

We estimated expected sensibility of the proposed measurement for observation of the X rays from the transition  $(4, 3) \rightarrow (3, 2)$  and  $(3, 2) \rightarrow (2, 1)$  of  $\Xi^-$  C atoms in the phase-1 data taking, with the number of  $K^-$  beams expected in J-PARC E70. Figure 8 shows expected X-ray energy spectra with the phase-1 statistics. The background in the X-ray spectrum is estimated based on data of a test experiment for J-PARC E03 [2018] in which the background level was studied with actual detectors and beams by selecting the  $(K^-, K^+)$  reaction by KURAMA spectrometer. Measured background level in the

test experiment is scaled for difference of an acceptance of Ge detectors and a number of beams. The spectrum (a) corresponds to the transition  $(4, 3) \rightarrow (3, 2)$  of which the energy width is expected to be match smaller than our detector resolution. Peak structure can be observed with the phase-1 statistics. On the other hand, sensitivity for the X rays of the transition  $(3, 2) \rightarrow (2, 1)$  will be much affected by the the absorption strength. We have a chance to obtain peak structure with the phase-1 statistics if branching ratio of X rays from the  $(3, 2)$  state is higher than 50% and the energy width is lower than 2 keV as shown in Fig.8 (b) and (c). An accuracy for the energy shift  $\sigma(\Delta E)$  of the transition  $(4, 3) \rightarrow (3, 2)$  is expected to be  $\sigma(\Delta E) = 0.4$  keV, assuming a negligible small energy width ( $\Gamma$ ) than the detector resolution. For the transition  $(3, 2) \rightarrow (2, 1)$ ,  $\sigma(\Delta E) = 0.5$  keV and 1 keV if  $\Gamma = 0$  keV and 2 keV, respectively.

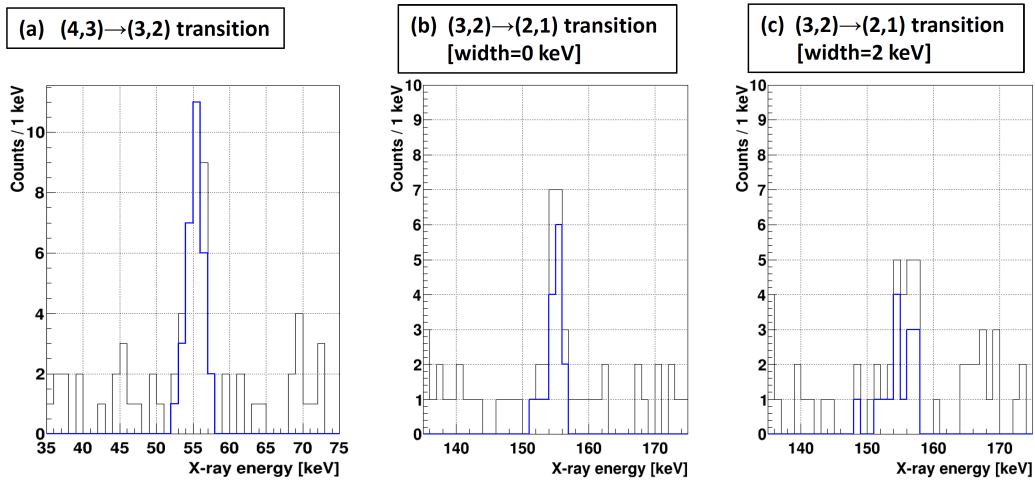


Figure 8: Expected X-ray energy spectrum (a) for the transition  $(4, 3) \rightarrow (3, 2)$  and (b) for the transition  $(3, 2) \rightarrow (2, 1)$  with no natural width. (c) is the same as (b) with a width of 2 keV.

Because accuracies for the energy shift and the width is not sufficient and sensitivity seems to be low for the case of the width of more than 2 keV with a number of  $K^-$  beams expected in J-PARC E70, we will request additional beam time as phase-2 after the phase-1 data taking. For a case study, the sensitivity with three times higher statistics, corresponding to additional twice beam time than J-PARC E70 in the phase-2, is estimated with same condition as the phase-1. An accuracies for the energy shift  $\sigma(\Delta E)$  for the transition  $(4, 3) \rightarrow (3, 2)$  is expected to be  $\sigma(\Delta E) = 0.2$  keV. For the transition  $(3, 2) \rightarrow (2, 1)$ ,  $\sigma(\Delta E) = 0.3$  keV and 0.6 keV if  $\Gamma = 0$  keV and 2 keV, respectively. In addition, it is possible to observe the transition  $(3, 2) \rightarrow (2, 1)$  even if the width is 4 keV. As already mentioned, there are large uncertainties on this yield estimation because of uncertainties on the theoretical calculation and unknown absorption strength which affect both the yield and the energy width. Therefore, we will reconsider about necessary

statistics for the phase-2 data taking based on an analysis of the phase-1 data.

## 5 Summary

X-ray spectroscopy of hadronic atoms is a powerful tool to investigate strong interaction between the hadron and nuclei. No experimental data for  $\Xi$ -atomic X ray exists at present. We are aiming for measurement of X rays from  $\Xi^-$  atoms on various target nuclei over wide mass range. In this proposed experiment, a carbon target was selected because of a technical reason and an additional motivation. We have conducted the first experiment for  $\Xi^-$  C atomic X-ray spectroscopy in J-PARC E07 and found no clear peak structure because of technical limitations. The sensitivity will be improved in the proposed experiment by introducing an Active Fiber Target (AFT) system which will be used in J-PARC E70, expected to be run in 2023. We are planning phase-1 data-taking for the X-ray spectroscopy in parallel with J-PARC E70 using S-2S spectrometer, AFT and modified Hyperball-X. Expected beam time for physics run is 20 days (common with J-PARC E70) assuming 83kW MR operation as requested by the J-PARC E70 collaboration. For the X-ray spectroscopy, additional  $\sim 1$  day commissioning beam time is necessary for the modified Hyperball-X just before the physics run, while commissioning for other apparatus is common with E70. Two X-ray transitions will be observed with the phase-1 statistics. However, there are uncertainties on the yield estimation of X rays and the energy width. We will reconsider about necessary statistics for the phase-2 data-taking to obtain sufficient accuracy for the energy shifts and widths.

## References

- [1] M. Yoshimoto *et al.*, PTEP 2021 (2021) 7, 073D02.
- [2] P. Khaustov *et al.*, Phys. Rev. C 61, 054603 (2000).
- [3] T. Nagae *et al.*, AIP Conf. Proc. 2130 (2019) 1, 020015.
- [4] H. Ekawa *et al.*, PTEP 2019 (2019) 2, 021D02.
- [5] S.H. Hayakawa *et al.*, Phys. Rev. Lett. 126 (2021) 6, 062501.
- [6] S. Acharya *et al.*, Phys. Rev. Lett. 123 (2019), 112002.
- [7] M. M. Nagels *et al.*, Phys. Rev. C 99 (2019) 044003.
- [8] K. Sasaki *et al.*, Nucl. Phys. A 998 (2020) 121737.
- [9] M. Kohno, Phys. Rev. C 100, 024313 (2019).

- [10] M. M. Nagels *et al.*, Phys. Rev. D 15 (1977) 2547.
- [11] M. Yamaguchi *et al.*, Prog. Thoer. Phys. 105 (2001) 627.
- [12] Th. A. Rijken and Y. Yamamoto, Phys. Rev. C 73 (2006) 044008.
- [13] E. Friedman, A. Gal, the International School of Physics Enrico Fermi (2007).
- [14] T. Koie, private communication (2020).
- [15] H. Takahashi *et al.*, Phys. Rev. Lett. 87 (2001) 212502.
- [16] T. Nagae *et al.*, J-PARC E70 technical design report (2019).
- [17] M. Fujita, Doctoral thesis, Tohoku University (2019).
- [18] T. Takahashi *et al.*, PTEP 2012 (2012) 02B010.
- [19] R. Honda *et al.*, Phys. Rev. C96 (2017) no.1, 014005.
- [20] Y. Igarashi *et al.*, IEEE Trans. Nucl. Sci. 57, 618 (2010).
- [21] T. Iijima *et al.*, Nucl. Phys. A546 (1992) 588.

## Appendix:

### Previous $\Xi^-$ -atomic X-ray spectroscopy at J-PARC

No experimental data for  $\Xi$ -atomic X ray exists at present. We are aiming for the world-first detection of the X rays and have conducted two experiments, J-PARC E07(2016-2017) and J-PARC E03(2020-2021). Preliminary reports from these experiments are shown below.

#### A.1 measurement for $\Xi^-$ atoms on C, Br and Ag in J-PARC E07

Our first measurement on  $\Xi$ -atomic X rays has been performed as a byproduct of J-PARC E07 experiment, search for double  $\Lambda$  hypernuclei and  $\Xi$  hypernuclei with hybrid emulsion technique. The data taking was done in 2016-2017. Figure 9(a) shows experimental setup near the target. In this experiment, hypernuclei were produced via  $\Xi^-$  capture by nuclei in a emulsion stack.  $\Xi^-$ s were produced via the  $(K^-, K^+)$  reaction and injected into the emulsion. Stopped  $\Xi^-$ s should form  $\Xi$  atoms before the hypernuclear production reaction. Tracks of  $\Xi^-$ , measured by KURAMA spectrometer, were used for a track following procedure for emulsion analysis. By applying this method, called hybrid emulsion technique, we found  $\Xi^-$  stop events efficiently.

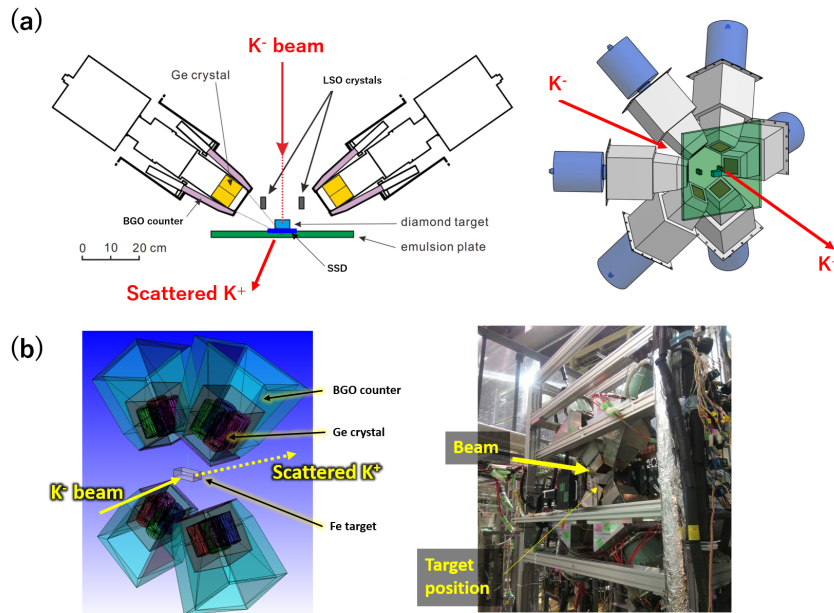


Figure 9: Experimental setup near the target in (a) J-PARC E07 and (b) J-PARC E03.

For the X-ray measurement, a germanium(Ge) detector array, Hyperball-X, was installed near the emulsion stack. The array can mount six detector units which consist of

a Ge detector and BGO suppressors. When  $\Xi^-$ s stop in emulsion, it is possible to form  $\Xi$  atoms on nuclei contained in the emulsion: C, O, N, O, Br and Ag. It is noted that yields of  $\Xi$  atoms on Ag and Br are expected to be large because  $\Xi^-$  will mostly captured by heavy nuclei. In addition,  $\Xi^-$  can stop inside the  $\Xi^-$  production target, a 3.2 g/cm<sup>2</sup> thick diamond.  $\Xi^-$  C atoms can be formed in such a event. In this measurement, we applied two methods to observe  $\Xi$ -atomic X rays; (1) combined analysis with  $\Xi^-$  stop identification using emulsion information, and (2) coincidence with tagging only  $\Xi^-$  production without emulsion information.

### Combined analysis with emulsion information

By selecting  $\Xi^-$  stop events with emulsion information, a good signal to noise ratio on the X-ray spectrum is expected while yield should be low because of a low  $\Xi^-$  stopping probability and low abundances of each target nucleus in the emulsion: C, N, O, Br and Ag. Furthermore, a solid angle for Ge detectors was limited by interferences with the emulsion and tracking system. As already mentioned,  $\Xi^-$  atoms on Br and Ag are expected to be seen in X-ray spectra with this method. Expected X-ray transitions from "last"  $\Xi^-$ -atomic states, which have the highest absorption probability per formation of  $\Xi^-$  atoms, are  $(n, l) = (7, 6) \rightarrow (6, 5)$  for Br and  $(8, 7) \rightarrow (7, 6)$  for Ag. Corresponding X-ray energies are 315 and 370 keV, respectively. At present, the emulsion analysis is ongoing and a number of available  $\Xi^-$  stop events is about 20% of full statistics. It is difficult to see peak structure in the X-ray spectrum because expected X-ray counts is  $\sim 4$  with this statistics. Further progress in emulsion analysis is awaited for more  $\Xi^-$  stop events.

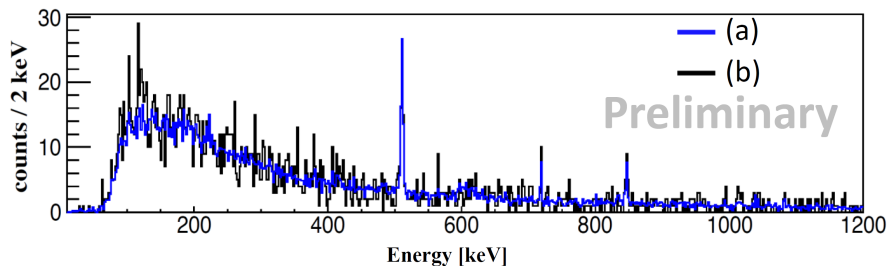


Figure 10: X-ray energy spectrum obtained in J-PARC E07 by an analysis without emulsion information [17]. The spectrum (a) for the events in coincidence with  $\Xi^-$  production is scaled. The spectrum (b) for the events in coincidence with  $\Xi^-$  having a large stop probability in the target.

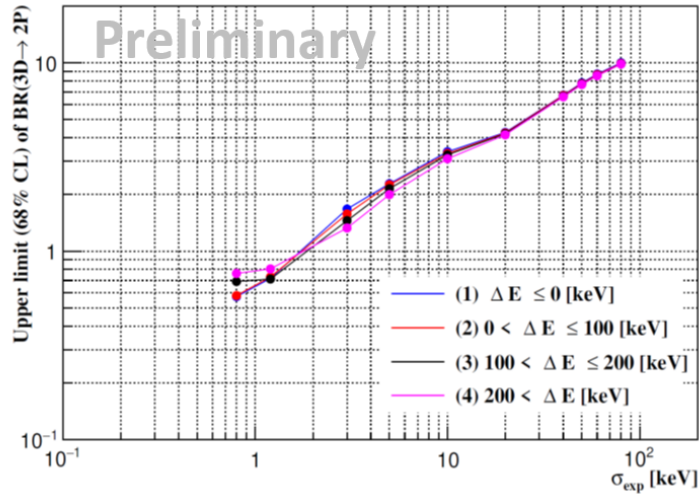


Figure 11: Upper limit of the branching ratio of  $(3, 2) \rightarrow (2, 1)$  transition of  $\Xi^-$  C atoms obtained in J-PARC E07 as a function of the X-ray peak width [17]. The upper limit of branching ratio was evaluated in the each energy region.

### Analysis without emulsion information

$\Xi^-$  C atoms can be formed when produced  $\Xi^-$ s stop in the diamond target. In this analysis, we tried to select events in which  $\Xi^-$ s not reach to a SSD placed at just downstream of the diamond target. In addition, by selecting low recoil momentum  $\Xi^-$ s, true X-ray events will be selected efficiently due to a high stop probability. However, a signal to noise ratio is lower than the emulsion combined analysis in which  $\Xi^-$  stop events are clearly identified. The expected X-ray transition from "last"  $\Xi^-$  C atomic state is  $(3, 2) \rightarrow (2, 1)$ , of which corresponding X-ray energy is 155 keV. Unlike in the previous method, the full statistics is available without the emulsion analysis. Figure 10 shows preliminary result of X-ray spectrum, where no clear peak structure was observed. We estimated a upper limit for the X-ray yield of the  $(3, 2) \rightarrow (2, 1)$  transition to be  $\sim 40\%$  /  $\Xi^-$  stop assuming 1 keV peak width in the energy region of 100-200 keV as shown in Fig. 11. This limit is close to a value suggested by a theoretical case study with the lattice QCD potential [14]. In this proposed experiment, we will re-try this measurement with an improved sensitivity.

## A.2 $\Xi^-$ Fe atom measurement in J-PARC E03

Our second measurement on  $\Xi^-$ -atomic X rays has been performed in J-PARC E03 which is dedicated experiment for the X-ray spectroscopy. We selected Iron as a target because of (1) technical reason; Iron is enough dense ( $7.9 \text{ g/cm}^3$ ) for a higher  $\Xi^-$  stopping probability and (2) physical reason; the expected absorption strength corresponding to

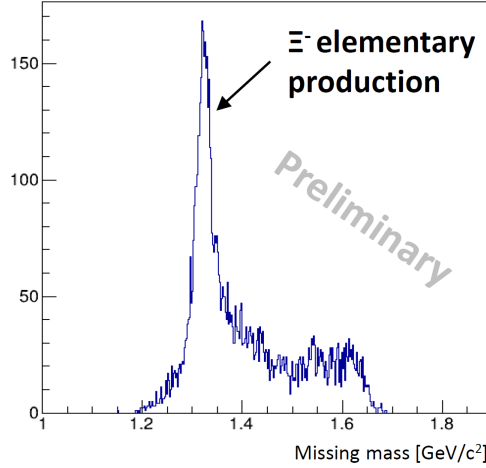


Figure 12: Missing-mass spectrum for the  $p(K^-, K^+)X$  reaction with  $\text{CH}_2$  target obtained in J-PARC E03 with KURAMA spectrometer.

the energy width of 4 keV is suitable for our measurement. This energy width is suggested in theoretical calculation assuming strong absorption with a W.S. shape optical potential of  $-24 - 3i$  MeV. On the other hand, recent lattice QCD calculation shows more than one order of magnitude smaller imaginary strength. A sharp peak structure in X-ray spectrum will be seen in such a weak absorption case. We decided to run with 10% statistics (1<sup>st</sup>-phase) of the original proposal for not full accelerator intensity. With 1<sup>st</sup>-phase statistics, it is expected that a peak structure of the X-ray transition from "last"  $\Xi^-$  Fe atomic state,  $(6, 5) \rightarrow (5, 4)$  transition of which corresponding energy is  $\sim 286$  keV, can be seen if the energy width is 1 keV, while full statistics is necessary in the case of 4 keV energy width. Furthermore, the upper X-ray transition,  $(7, 6) \rightarrow (6, 5)$  transition with corresponding energy of 172 keV, will be observed without peak broadening due to the energy width. The ratio between yields of the upper and the lower X-ray transition gives information of the absorption strength.

In this measurement,  $\Xi^-$ s were produced by the  $(K^-, K^+)$  reaction in a  $24 \text{ g/cm}^2$  thick Iron target and stopped in it.  $\Xi^-$  productions were tagged by the missing mass analysis by reconstructing momenta of beam  $K^-$ s and scattered  $K^+$ s with magnetic spectrometers: K1.8 Beamline spectrometer and KURAMA spectrometer. X rays were detected by a Ge detector array by taking a coincidence with magnetic spectrometers. The Ge detector array Hyperball-X' was installed near the target as shown in Fig.9(b), instead of another Ge detector array Hyperball-J which will be used for the full statistics run. Hyperball-X' consists of four Ge + BGO suppressor units with a vertically covering configuration to avoid self-absorption of X rays inside the horizontally wide Iron target. Clover-type Ge detectors were mounted to the array for a large solid angle and a low counting rate of each Ge crystal. High energy resolution has great merit for the 1 keV energy width case,

even if dead time due to signal pileups become longer. An energy resolution was  $\sim 2.3$  keV (FWHM) for 307 keV.

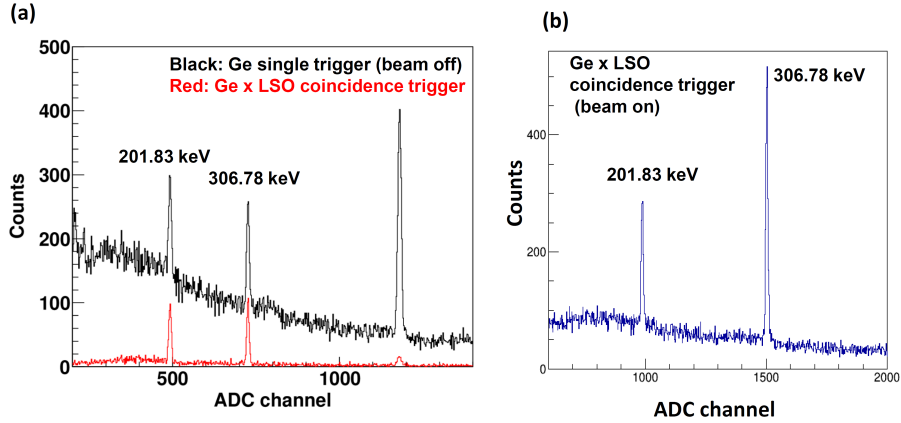


Figure 13: Energy spectra of Ge detector for energy calibration. (a) is that of with (red) and without (black) the Ge and LSO coincidence trigger. (b) is that taken in beam on period using the trigger.

The data taking for the E03 1<sup>st</sup>-phase was done in Apr. 2021 with total irradiated  $K^-$  beams of  $9.5 \times 10^{10}$ . An analysis is on-going for selecting the  $(K^-, K^+)$  reaction and detecting X rays. We confirmed that  $\Xi^-$  production events can be clearly tagged by the missing mass method as shown in Fig.12 with momentum reconstructions in Beam-line spectrometer and KURAMA spectrometer. Performances of Hyperball-X' were also evaluated for resolutions, efficiencies and background suppression. In addition, with the "LSO pulser" described in section 3.3, an energy calibration accuracy of 0.05 keV was achieved by taking In-beam calibration data as shown in Fig.13(b), where clear reference peaks can be obtained even in the beam on period. After finalizing the analysis of this data, we will report results in near future.